BIOENGINEERING

Skin-like biosensor system via electrochemical channels for noninvasive blood glucose monitoring

Yihao Chen,[1,2] Siyuan Lu,[1,2] Shasha Zhang,[3] Yan Li,[1,2] Zhe Qu,[1,2] Ying Chen,[1,2] Bingwei Lu,[1,2] Xinyan Wang,[3] Xue Feng[1,2]*

Currently, noninvasive glucose monitoring is not widely appreciated because of its uncertain measurement accuracy, weak blood glucose correlation, and inability to detect hyperglycemia/hypoglycemia during sleep. We present a strategy to design and fabricate a skin-like biosensor system for noninvasive, in situ, and highly accurate intravascular blood glucose monitoring. The system integrates an ultrathin skin-like biosensor with paper battery–powered electrochemical twin channels (ETCs). The designed subcutaneous ETCs drive intravascular blood glucose out of the vessel and transport it to the skin surface. The ultrathin (~3 μm) nanostructured biosensor, with high sensitivity (130.4 μA/mM), fully absorbs and measures the glucose, owing to its extreme conformability. We conducted in vivo human clinical trials. The noninvasive measurement results for intravascular blood glucose showed a high correlation (>0.9) with clinically measured blood glucose levels. The system opens up new prospects for clinical-grade noninvasive continuous glucose monitoring.

INTRODUCTION

Diabetes is a worldwide chronic disease that threatens human health and lives (*1*, *2*). The World Health Organization has reported that nearly 422 million adults were diagnosed with diabetes in 2014. Millions of people have lost their lives because of poorly controlled blood glucose. Regulated and continuous glucose monitoring (CGM) of diabetes patients can provide better monitoring and control of blood glucose and prevent complications (fig. S1). Glucose monitoring with commercially available products relies on invasive lancet approaches. Repeated finger pricks not only hinder patient compliance because of pain but also result in skin irritation and bacterial infections.

Researchers have performed numerous studies regarding noninvasive glucose monitoring (*3*–*5*). Optical measurements such as infrared spectroscopy, optical coherence tomography, and fluorescence (*6*–*8*) are easily affected by interference from confounding factors. Indirect measurements using metabolic heat, Raman spectroscopy, impedance, and polarization changes (*9*–*11*) lack specificity for glucose. Body fluids such as sweat, saliva, and tears are potential candidates for direct glucose measurement (*12*–*18*). However, the density of glucose in those fluids is only 1 to 10% of that in the blood. Thus, the correlation with blood glucose levels cannot be guaranteed. In addition, body fluid glucose measurement accuracy decreases because of water evaporation, seasonal fluid volume changes, and other internal components. Repeated and forced "sampling" (for instance, sweating) is not suitable for continuous, long-term, and during-sleep monitoring. As compared with the above methods, measuring the glucose in interstitial fluid (ISF) is more promising. The methods for sampling ISF are ultrasound, laser technology, and reverse iontophoresis (*19*–*21*). Although reverse iontophoresis is the most prevalent among these methods, it is scarcely recognized by physicians before the blood glucose correlations are further improved. In addition, the use of a high-density current and a long warm-up time often induces skin irritation and pain in users (*22*–*24*).

[1]AML, Department of Engineering Mechanics, Tsinghua University, Beijing 100084, China. [2]Center for Flexible Electronics Technology, Tsinghua University, Beijing 100084, China. [3]Special Diagnosis Department, People's Liberation Army Air Force General Hospital, Beijing 100142, China.
*Corresponding author. Email: fengxue@tsinghua.edu.cn

RESULTS

Noninvasive intravascular glucose measuring principle and the skin-like biosensors

Here, we present a strategy for a fully noninvasive biosensor system for intravascular blood glucose monitoring. The system consists of a flexible biocompatible paper battery and ultrathin skin-like biosensors. The paper battery (Fig. 1B) is first attached to the skin to generate subcutaneous electrochemical twin channels (ETCs) (Fig. 1A and fig. S2). The ETCs act through hyaluronic acid (HA) penetration into the ISF (anode channel), intravascular blood glucose refiltration from vessels, and glucose reverse iontophoresis to the skin surface (cathode channel) (Fig. 1A). Under the paper battery anode, high-density positively charged HA is transdermally repelled into the ISF. Extra HA increases the ISF osmotic pressure and breaks the balance between ISF filtration and reabsorption, thus promoting intravascular blood glucose refiltration at the arterial ends and reducing the reabsorption at the venous ends. A higher molar glucose concentration in the ISF also increases the flux of reverse iontophoresis in low-current occasions (*25*). As a result, more intravascular blood glucose is driven out of the vessel and is transported to the skin surface (fig. S3). The measurement of "real" blood glucose (that is, the glucose previously existed in the blood together with the glucose previously in the ISF) greatly improves the blood glucose correlation.

Next, the ultrathin skin-like biosensors completely conform to the skin and measure the outward-transported glucose driven by ETCs. These biosensors are multilayered with "sand dune" nanostructures, which exhibit better electrochemical properties and higher sensitivity (Fig. 1C and fig. S4). The layers of the biosensor, from bottom to top, are polymethyl methacrylate (PMMA) (80 nm), polyimide (PI) (1.6 μm), a nanostructured deposited gold thin film (100 nm), an electrochemically deposited nanometer transducer layer (51.8 nm), and a transfer/glucose oxidase (GOx) immobilization layer (~1 μm). We first fabricate the biosensors on the silicon wafers with various shapes (fig. S5) and then transfer-printed (*26*–*28*) them by bionic "capillary grabbing." The transfer-printed biosensors are ultrathin, skin-like, and flexible (Fig. 1D, left). The total thickness of the multilayer biosensor is approximately 3 μm so that the biosensor fully conforms to the skin with intimate contact (Fig. 1D, right). The conformal contact with dermal ridges increases the contact areas between the biosensor and outward-transported

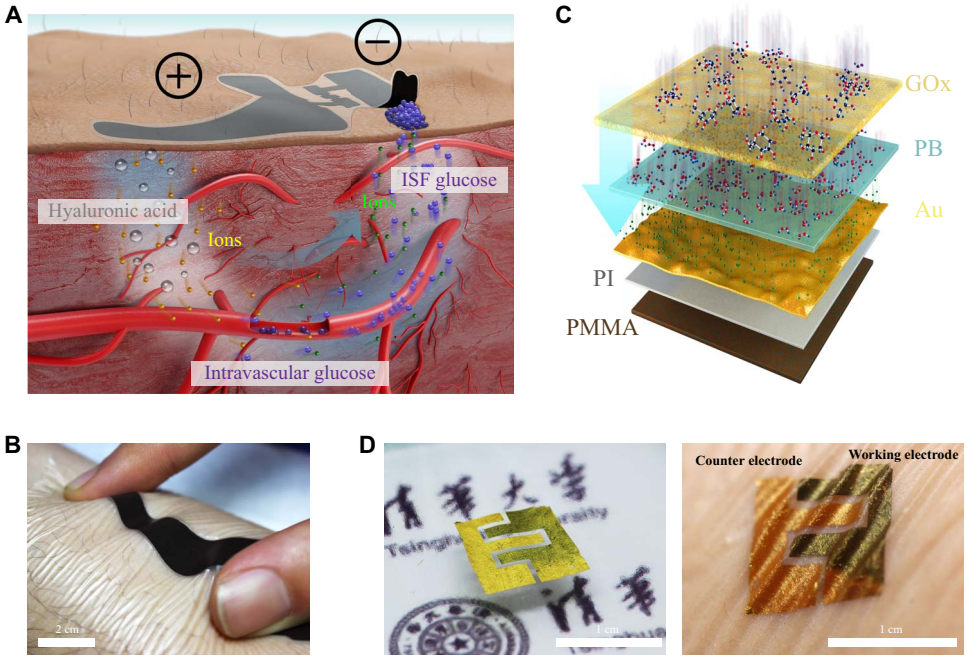

Fig. 1. ETC principle and the skin-like biosensors. (**A**) Schematic of the ETCs, which perform HA penetration, glucose refiltration, and glucose outward transportation. (**B**) Schematic of the ultrathin skin-like biosensor multilayers. (**C**) Thin, flexible, and biocompatible paper battery attached to the skin surface for ETC measurement. (**D**) Selective electrochemically deposited dual electrodes of the biosensors (left). The biosensor completely conforms to the skin surface (right).

glucose on the skin (*29*). A larger surface energy reinforces the absorption of glucose on the biosensor surface. As a result, we can collect more glucose and measure it by such biosensors, thereby improving the measurement accuracy and signal-to-noise ratio of in vivo measurements (*30*).

Electrochemical and mechanical characterization of the device

We designed the biosensor as a "two-electrode system" (a working electrode and a counter electrode) in the in vivo measurements. The very small reaction current measurement condition could guarantee the electrochemical measurement accuracy. The dual electrodes were fabricated and patterned simultaneously but modified selectively via the insulation across the two electrodes. For the Prussian blue (PB) transducer layer electrochemical deposition (ECD) on the deposited nanometer gold electrode, a shorter deposition time yields a thinner PB thin film, which is more flexible (fig. S6) and has a lower ion diffusion resistance. However, the PB thin film that was electrochemically deposited on the original gold electrode (O-PB) (Fig. 2A, left) cracked easily during short (for example, 15 s) deposition (Fig. 2A, right, and fig. S7), thus showing that the thin film was fragile and the adhesion to the electrode was weak (fig. S8). To obtain nanometer-thick and high-quality PB thin films, we fabricated the sand dune nanostructures on the surface of the gold electrode before ECD (Fig.2B, left). The PB thin film deposited on the nanostructured gold electrode (N-PB) was uniform and complete (Fig. 2B, right) with a thickness of approximately 51.8 nm (fig. S9).

Nanostructured gold (N-Au) is better for nano-PB deposition than original gold (O-Au) because of the greater number of defects and larger surface area, which facilitate particle deposition and thin film growth. Using numerical simulations, we further studied other advantages of the nanostructures. The consumption of solutes during deposition formed an ion density gradient in the microreaction pool, inducing inner flow and ion transfer over the electrode surface (Fig. 2C, left, and fig. S8). As shown in the results of fluid mechanics simulations, surface nanostructures largely increase the flow velocity over the electrode (Fig. 2C, right, top). A higher flow rate facilitates ion replenishment during deposition, increasing the deposition rate. The thin film growth rate is higher on nanostructured surfaces in the simulation of the ECD (Fig. 2C, right, bottom). In the ECD of PB, the deposition current of N-Au was nearly three times larger than that of O-Au (Fig. 2D) for the same experimental parameters. In the cyclic voltammetry (CV) scan, O-PB and N-PB had similar redox voltages, whereas the redox current of N-PB (Fig. 2E) was more than five times higher than that of O-PB (Fig. 2E, inset), thus indicating better redox performance. Moreover, the N-PB exhibited excellent stability after 20 scan cycles (fig. S10). In an electrochemical impedance spectroscopy (EIS) analysis, N-PB demonstrated lower diffusion resistance than O-PB, owing to its larger active surface areas (Fig. 2F and fig. S11). Besides nanostructures, the resistance was further decreased in thinner N-PB. Three N-PB thin films with different thicknesses (deposition times: 15 s, 90 s, and 10 min) were compared for the response to the same density of hydrogen peroxide (H_2O_2). The response of the thinner N-PB thin film was greater and faster (Fig. 2G). In time stability tests, the CV properties of N-PB did not change after 2 months of storage at room temperature (Fig. 2H and fig. S12).

We characterized the mechanical properties of O-PB and N-PB by nanoindenters (fig. S13). The Young's modulus and hardness of N-PB were smaller than those of O-PB (Fig. 2I), thus indicating that the former has smaller grain sizes, fewer defects, and lesser lattice distortion even for a higher deposition speed and with a shorter deposition time. The grain stress concentration largely decreased, thus making the nanometer N-PB thin film firm and unbreakable.

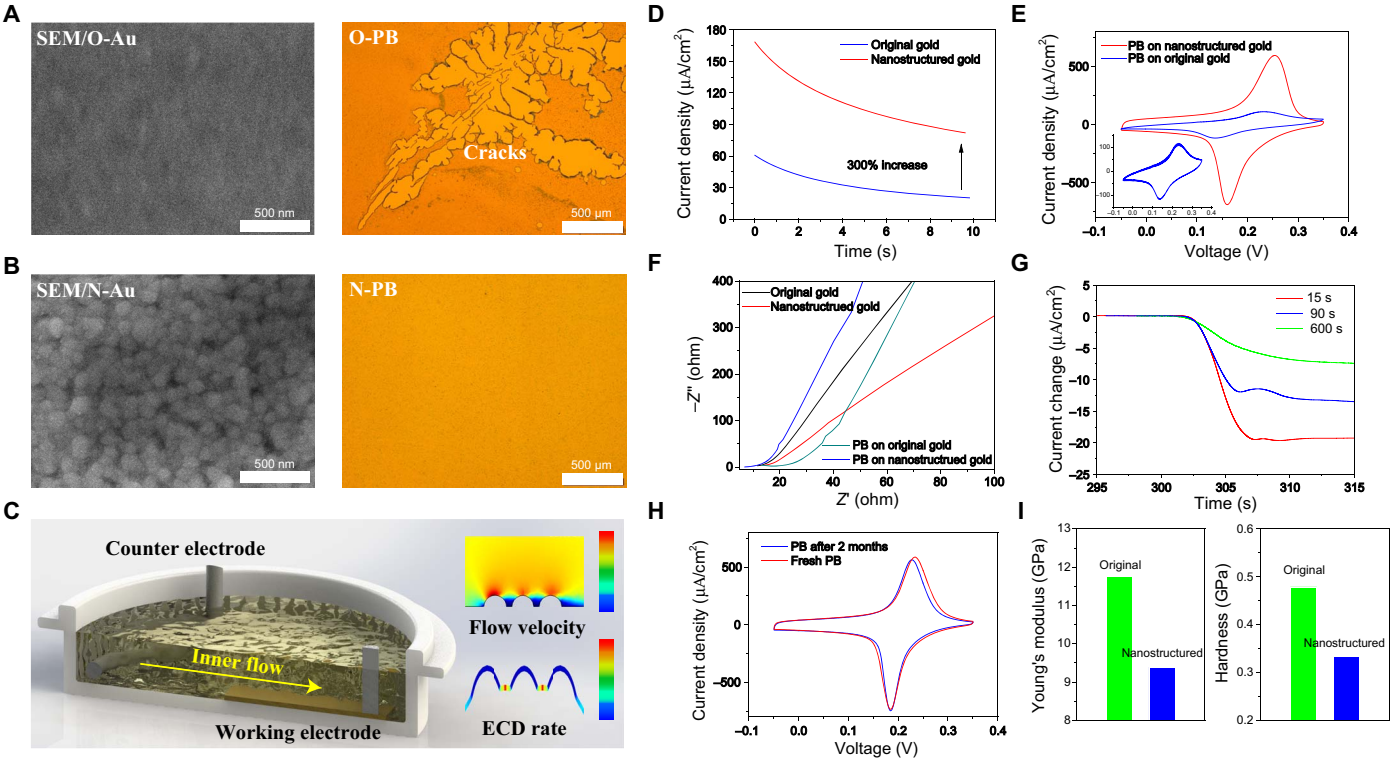

Fig. 2. Electrochemical and mechanical characterization of the device. (**A**) Scanning electron microscopy (SEM) micrograph of O-Au (left) and optical micrograph of broken O-PB (right). (**B**) SEM micrograph of N-Au (left) and optical micrograph of complete N-PB (right). (**C**) Schematic of surface nanostructure–induced inner flow during ECD (left). Fluid mechanics simulation of the velocity distribution when the inner flow passes over the surface of the nanostructure (right, top) and electrochemical simulation of the growth rate of PB during ECD on N-Au (right, bottom). (**D**) Deposition current of O-PB (blue) and N-PB (red). (**E**) CV scan of O-PB (blue) and N-PB (red). (Inset) CV curve of O-PB (−0.05 to 0.35 V versus Ag/AgCl reference electrode at a scan rate of 50 mV/s). (**F**) Nyquist plot of EIS of O-Au (black), N-Au (red), O-PB (green), and N-PB (blue). (**G**) Response of N-PB to the same density H_2O_2 as a function of deposition time (that is, thickness). (**H**) CV of freshly deposited N-PB and N-PB after 2 months of storage. (**I**) Young's modulus and hardness of N-PB (blue) and O-PB (green).

Bionic transfer printing and glucose measurement calibration

To achieve perfect skin conformability and higher measurement accuracy, thinner biosensors are desirable. PI is spin-coated and cured on the silicon wafer as the substrate before the electrode fabrication and PB deposition. Compared with ready-made commercial polymer thin films, this coating has a smaller thickness (1.6 μm), higher fabrication accuracy (0.7 μm), and better surface conditions. After ECD, the greatest challenge is how to pick up the ultrathin but fragile biosensor from the substrate while retaining both the shape and function.

Inspired by the "Rose of Bethlehem" in the Israeli desert, we used bionic "ROSE" (rising oriented stickiness evaporation) for the biosensor transfer printing. We performed the ROSE by using only drops of chitosan solution containing GOx (Fig. 3A). Thus, we achieved the transfer printing and enzyme immobilization process simultaneously. The transfer began with dropping the sticky solution on the surface of the on-wafer fabricated device. As the solvent evaporated, the drop became smaller while the drop's edges remained fixed. When the drop started to form a thin film, the resulting capillary force grabbed and rose up biosensor edges. The delamination of the biosensor from the wafer spread inwardly, eventually picking up the entire biosensor thin film from the wafer (movie S1). With the help of ROSE, biosensors with different patterns can be automatically transferred (Fig. 3B). After the biosensor was ROSE-transferred, we performed a CV scan for comparison with the results before transfer printing (Fig. 3C). The redox voltages and currents differed only slightly from the pretransfer test values, thus showing that the PB transducer layer and the gold electrode were still complete and functional.

After transfer printing and enzyme immobilization, we characterized the biosensor's responses to different glucose densities (Fig. 3, D and E). The glucose biosensing sensitivity of the low-density range (5 to 35 μM) was 130.4 μA/mM (Fig. 3D, inset), that of the moderate-density range (50 to 100 μM) was 158.0 μA/mM (Fig. 3E, inset), and that of the high-density range is 196.3 μA/mM (fig. S14). The biosensor's responses and CV characterizations remained stable in repeated experiments (Fig. 3F and fig. S15). The biosensor was more selective for glucose than other skin interference components (Fig. 3G). Although temperature and pH changes affected the biosensor response (fig. S16), the interference induced by water evaporation and residuals can be minimized because we used the ISF instead of other fluids (for example, sweat and tears) for the measurement. Generally, the skin surface temperature fluctuates by approximately 0.3°C at room temperature in a 20-min period of time (fig. S17), thus causing a measurement drift as small as 9 nA/cm^2.

Errors can be fully compensated by correcting the result with real-time and in situ skin temperature measurement. The nondeposited gold electrode acts as a linear resistance temperature sensor, with a temperature coefficient of resistance of 0.001/°C (Fig. 3H).

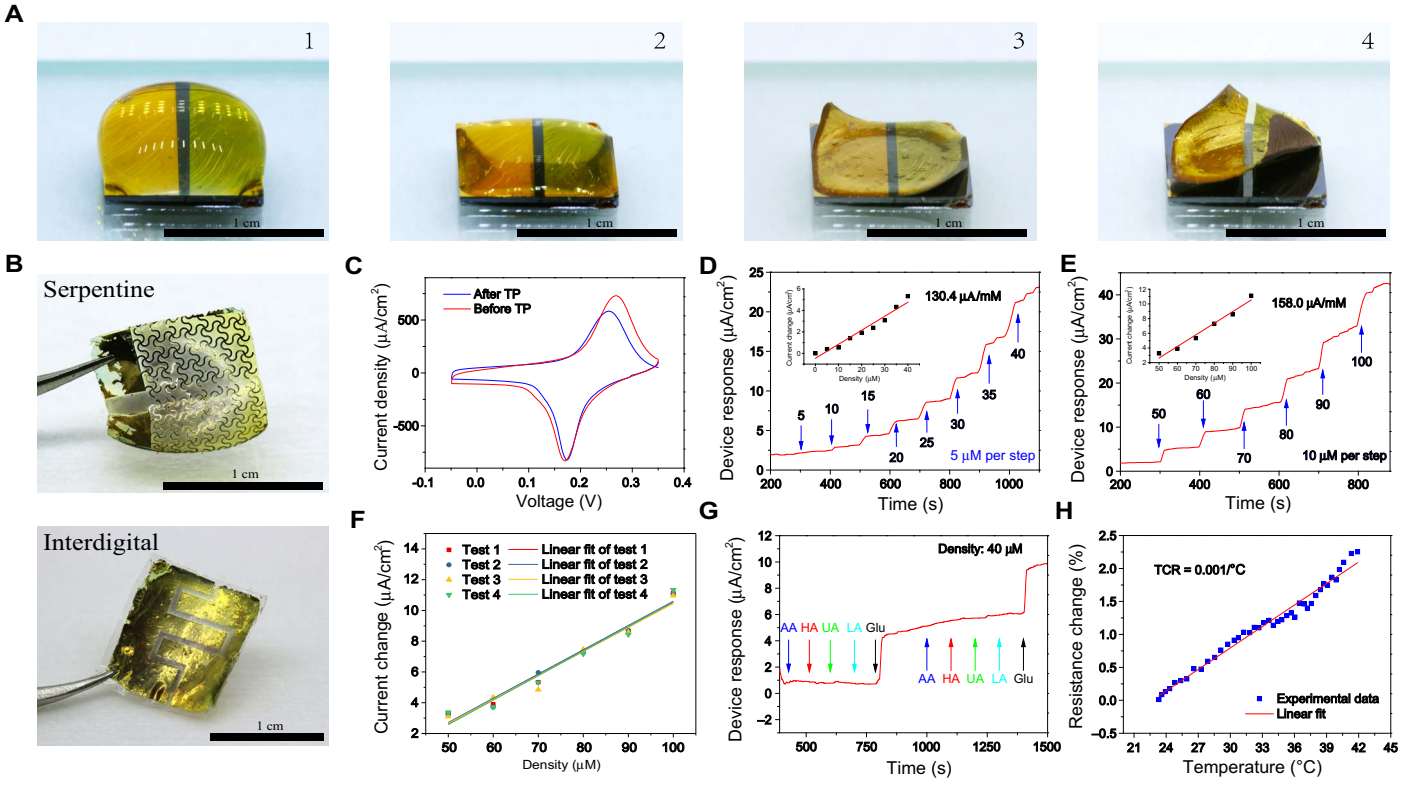

Fig. 3. Bionic transfer printing and glucose measurement calibration. (**A**) Process of bionic ROSE transfer printing. (**B**) Serpentine (top) and interdigital (bottom) pattern biosensors transfer-printed by ROSE. (**C**) CV of a biosensor before and after transfer printing (−0.05 to 0.35 V versus reference electrode at a scan rate of 50 mV/s). Amperometric *I-t* results of (**D**) low-density and (**E**) moderate-density glucose as measured in a calibration experiment. (Inset) Biosensor response as a function of density. (**F**) The glucose measurement response for 50 to 100 μM at 10 μM per step was repeated four times. (**G**) Amperometric *I-t* result of the selective response to glucose (Glu) and other interfering substances: ascorbic acid (AA), HA, uric acid (UA), and lactic acid (LA). (**H**) Temperature calibration result (TCR) of the temperature sensor.

In vivo clinical trials on human subjects

In in vivo clinical trials, we removed the paper battery after 20 min of ETC HA penetration and reverse iontophoresis process (Fig. 4A). Then, we firmly attached the ultrathin skin-like biosensor to the cathode-contacting area for skin surface glucose measurement (Fig. 1D, right). The biosensor response was shown by amperometric *I-t* curves (Fig. 4B).

The transport of the glucose in the reverse iontophoresis process is dominated by electroosmosis. The molar flux of the glucose is determined by the potential gradient across the skin and the molar concentration of the initial solute (*25*).

To verify the effect of ETCs, we performed an in vivo control test (with and without ETC HA penetration). The response of the biosensor with ETC HA penetration was much higher than that of the other biosensor, thus indicating that more glucose was transported from the vessel and ISF during the test (Fig. 4C). According to the theoretical analysis (Supplementary Text), the glucose density in the ISF was largely increased because of the HA-induced blood glucose filtration.

At the People's Liberation Army (PLA) Air Force General Hospital (China), we recruited three volunteers (one male and two females aged 24, 37, and 62 years) to participate in the in vivo clinical trials. None of the subjects had a medical history of heart disease. Subject 1 (male, 24 years old) and subject 2 (female, 37 years old) were healthy, whereas subject 3 (female, 62 years old) had type 2 diabetes. All the subjects were fully informed of the possible risks and provided with informed consent. Subject 1 measured his capillary blood glucose with finger-prick glucometer (Fig. 4D, left). Subjects 2 and 3 each underwent an oral glucose tolerance test (OGTT). With sampling through vein detained needles (Fig. 4D, right), the vein plasma blood levels of subjects 2 and 3 were measured with blood tests. All the subjects underwent noninvasive in vivo measurement with our ETC wearable devices at the same time as the blood sampling. During a 1-day period, subject 1's blood glucose was measured hourly with a clinically approved glucometer (ACCU-CHEK Performa, Roche) and the device during the time period 10:00 to 23:00. The results showed that the device measurement results (blue squares) matched well with the glucometer results (red dots), with a 1-hour time lag (Fig. 4E). The time lag was due to the ~20- to 30-min intrinsic density time lag (between glucose in ISF and blood) and the ~25-min measurement operation time. Increasing the reverse iontophoresis voltage and adjusting the correlated model could decrease the time lag. The statistical analysis showed that the two data groups had a high correlation coefficient of 0.915 ($P < 0.001$). For 5-day continuous monitoring, subject 1's blood glucose was measured daily at 08:00, 09:00, and 10:00 with the glucometer and the device (Fig. 4F). Considering the time lag, the glucometer measurement results were compared with the results from the device 1 hour earlier. The device measurement results correlated well with the glucometer results, with a high correlation coefficient of 0.900 ($P < 0.05$). For the OGTT, the correlation between the device measurement results and the blood test results was confirmed to have

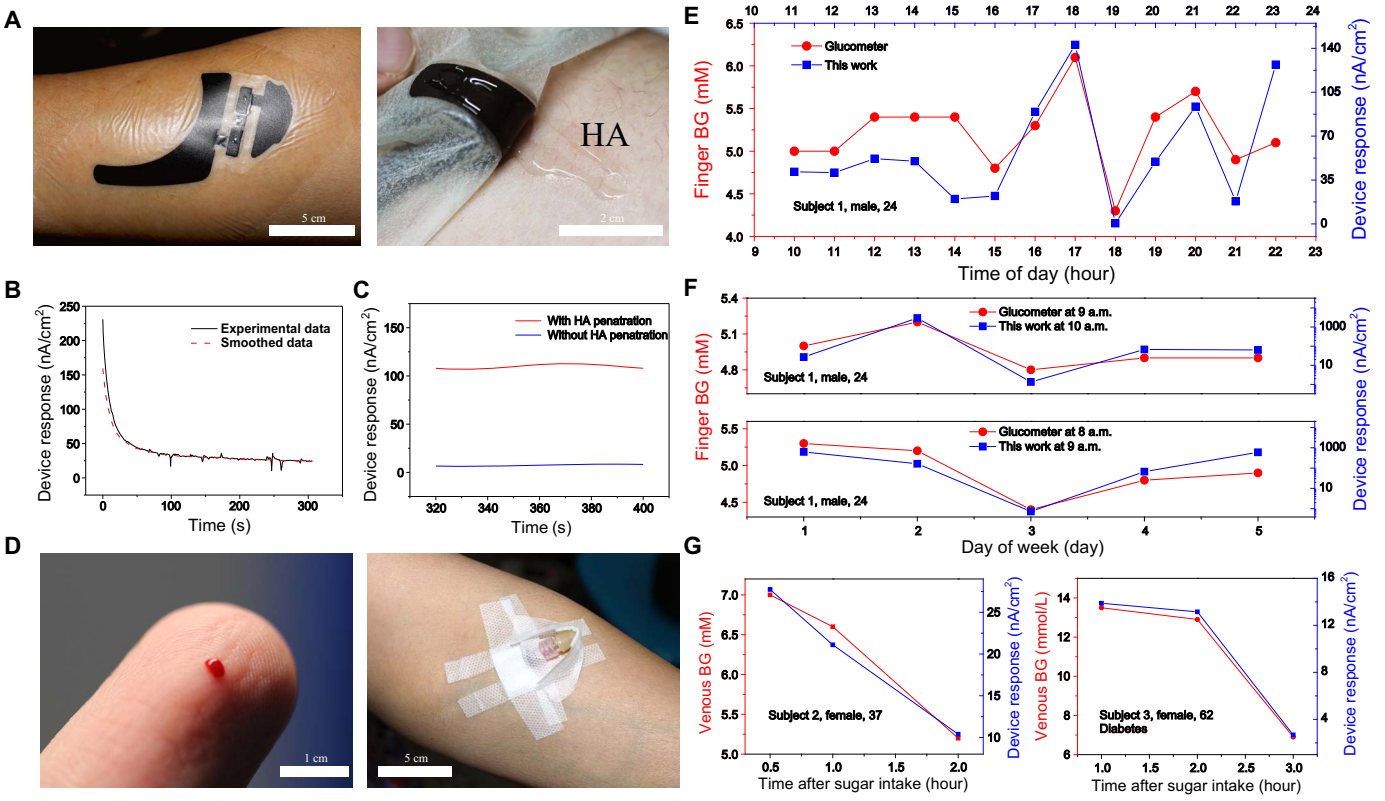

Fig. 4. In vivo clinical trials. (**A**) Paper battery being attached to the skin surface for ETC measurement (left), with HA sprayed under the paper battery anode (right). (**B**) Amperometric *I-t* result recorded from the biosensor attached to the skin surface. (**C**) Biosensing response current with (red) and without (blue) the ETC control test. (**D**) In vivo invasive blood glucose measurement by using a finger-prick glucometer (left) and a venous blood test with vein detained needles (right). (**E**) Results of hourly glucose monitoring in 1-day period from 10:00 to 23:00 by using a glucometer (red) and ETC devices (blue) (subject 1). (**F**) Results of 5-day glucose monitoring with the glucometer (red) and ETC devices (blue) (subject 1). (**G**) Results of blood glucose measured by using a plasma blood test with a vein detained needle (red) and ETC devices (blue) during the OGTT (subjects 2 and 3).

higher correlation coefficients of 0.9846 ($P < 0.02$) (subject 2) and 0.9997 ($P < 0.07$) (subject 3) (Fig. 4G). There were no signs or reports of irritation, pain, or inflammation on the skin surface for any of the subjects during and after the ETC device measurement (fig. S18).

DISCUSSION

The skin-like noninvasive blood glucose monitoring system measures the intravascular blood glucose and the glucose in ISF. The ETCs greatly improve the correlation between the noninvasive measurement results and the real blood glucose level. With proper calibration, the system is potentially suitable for medical-grade CGM and insulin therapy when working with micro-insulin pumps.

MATERIALS AND METHODS

Fabrication of the biosensor

Preparation of the silicon wafer

The silicon wafer was cleaned with acetone, deionized (DI) water, and isopropyl alcohol (IPA). The IPA was blown off with nitrogen. The silicon wafer was heated and dried using a heater at 120°C for 5 min.

Film making

A layer of PMMA (MicroChem) was spin-coated at 1500 rpm for 10 s and 3000 rpm for 30 s, and the PMMA film was cured at 180°C for 10 s. A layer of PI (PI-5J, Yidun) was spin-coated at 1500 rpm for 10 s and 3000 rpm for 30 s, and the PI film was cured at 80°C for 1 hour, 120°C for 1 hour, and 140°C for 1 hour.

Metal deposition and patterning

A layer of 10-nm Cr and 100-nm Au was deposited on the surface of the cured PI film with an electron beam. The silicon wafer was cut into 1 cm × 1 cm pieces. Au and Cr were photolithographed and etched into patterns such as interdigital and serpentine shapes.

Fabrication of gold surface nanostructure

The silicon wafer was dipped into the gold etchant ($KI + I + H_2O$) with the gold side down horizontally for 8 s. The gold surface was cleaned with DI water and blown dry.

Selective deposition of PB film on dual electrodes

The ECD aqueous solution was composed of with DI water, 2.5×10^{-3} M $FeCl_3$, 2.5×10^{-3}M $K_3[Fe(CN)_6]$, 0.1 M KCl, and 0.1 M HCl. The buffer aqueous solution was composed of DI water, 0.05 M KH_2PO_4, 0.05 M K_2HPO_4, and 0.1 M KCl. ECD was done in three-electrode system (fabricated working electrode, Ag/AgCl reference electrode, and Pt counter electrode) in a micro-electrochemical reaction pool (fig. S8). Deposition was done with potentiostatic polarization at 0.4 V versus reference electrode for 15 s by electrochemical workstation (CS300H, CorrTest Instruments).

Electrochemical characterization of the electrode

All the electrochemical characterizations were done on the electrochemical workstation. Voltage was set at −0.05 to 0.35 V versus reference

electrode at a scan rate of 50 mV/s in CV scans (Figs. 2, E and H, and 3C and figs. S10, S15, and S16B). EIS tests were swept from 1×10^{-2} to 1×10^{4} Hz (Fig. 2F and fig. S11). Response time test to H_2O_2 was done in *I-t* measurement with voltage set as 0 V versus reference electrode (Fig. 2G).

Mechanical characterization of the electrode

The mechanical property test was done on TriboIndenter (Ti-950, Hysitron). The indenter was pressed into the PB film to set the depth, and the load-displacement curve was recorded. The Young's modulus and hardness of the film were calculated from the curve.

Bionic ROSE transfer printing and enzyme immobilization

Preparing chitosan solution

An aqueous solution of 2% chitosan was prepared by dissolving chitosan powder into 2% acetic acid solution. The solution was stirred and heated to 80°C until chitosan completely dissolved. Glycerol (0.8%) was added and stirred evenly. The solution was placed at room temperature until it became clear without air bubbles.

Preparing GOx solution

GOx was resolved in DI water to prepare an aqueous enzyme solution of 34 mg/ml. The solution was placed at room temperature until it became clear without air bubbles.

Preparing the transfer print sticky solution

The chitosan solution was mixed with a GOx solution at a ratio of 1:1. The solution was stirred and placed at room temperature until it became clear without air bubbles.

Transferring and immobilization

Drops of sticky solution were dripped onto the surface of the wafer-based deposited PB and gold electrode before they flew out of the wafer. The device was placed horizontally at room temperature for 4 to 5 hours.

Electrochemical characterization of transferred PB

The transferred thin film device was coated on the silicon wafer, and CV scan (−0.05 to 0.35 V versus reference electrode at a scan rate of 50 mV/s) was performed in the buffer solution.

Calibration of glucose measurement

The device was measured in the buffer solution as working electrode, with Ag/AgCl as the reference electrode and Pt as the counter electrode. The device was calibrated with glucose solution density of three ranges. Low density ranges from 5 to 40 μM at a step of 5 μM every 100 s. Moderated density ranges from 50 to 100 μM at a step of 10 μM every 100 s. High density ranges from 150 to 225 μM at a step of 25 μM every 100 s. The response was recorded by amperometric *I-t* curve (0 V versus reference electrode). The fitting result of the current response as a function of glucose density was calculated by the current density increment (relative current change) of every glucose adding step.

pH and temperature influence test

The influence of the pH value of the buffer solution was tested with the buffer solution of different pH values (by adjusting the ratio of KH_2PO_4 and K_2HPO_4). Glucose response tests at 30, 35, and 40 μM were done in the buffer solution of pH 5.0, 5.68, and 6.18. Temperature influence test was done with a water bath. The device's response to the same density glucose was recorded in different temperature solutions.

Selectivity tests to other interferences

40 μM AA, 40 μM HA, 40 μM UA, 40 μM LA, and 40 μM glucose were added to the buffer solution in order twice. The amperometric *I-t* curve was recorded during the test (0 V versus reference electrode).

Temperature calibration of the temperature sensor

The device was placed in a water bath. The water bath was heated, and the water temperature was recorded with a Pt temperature sensor. The resistance of the gold temperature sensor in the device was recorded using a resistance meter (TH2515, Tonghui Electronic).

ETC measurement process

Preparation of the skin to be measured

Scrub scream was smeared to the skin surface and rubbed to remove dead skin on the epidermal layer. The scream and dead skin were washed with DI water. The water was wiped out and blown dry. Medical alcohol (75%) was used for sterilization. We waited until the alcohol evaporated completely.

Preparation of the paper battery to be used

The voltage of the paper battery (nominal voltage, 3 V; Power Paper Ltd.) was measured and checked to ensure that it is at the nominal voltage. The anode and cathode surface was cleaned with DI water, and the water was wiped out. High-density HA was dropped on the anode of the paper battery and spread evenly. The paper battery was attached to the prepared skin surface, covered, and fixed with waterproof and biocompatible film dressing (OPSITE FLEXIGRID, Smith & Nephew).

Glucose measurement with the biosensor

After 20 min, the film dressing and paper battery were removed from the skin surface. We firmly attached the biosensor to the cathode area for glucose measurement.

After-test treatment

The skin surface was washed with DI water and medical alcohol. The anode and cathode surface of the paper battery was washed with DI water.

In vivo glucose measurement experiment

Invasive glucose measurement was done using a commercial glucometer (ACCU-CHEK Performa, Roche) and vein detained needles.

Ethical approval for in vivo experiments

The in vivo experiments were done under the guidance and supervision of the PLA Air Force General Hospital. All procedures followed the guidelines of the International Review Board and were approved by the PLA Air Force General Hospital Medical Ethics Committee.

SUPPLEMENTARY MATERIALS

Supplementary material for this article is available at http://advances.sciencemag.org/cgi/content/full/3/12/e1701629/DC1

Supplementary Text

fig. S1. Advantage of CGM over prevalent glucose monitoring and treatment.

fig. S2. Thin and flexible biocompatible paper battery.

fig. S3. Schematic of high-density HA penetration promoting filtration of glucose in the blood.

fig. S4. Glucose biosensing principle.

fig. S5. Different patterns for glucose biosensing dual electrode.

fig. S6. Bending stiffness (that is, flexibility) as a function of device thickness.

fig. S7. SEM micrographs of electrochemical deposited PB on different gold electrodes.

fig. S8. PB sediments after the ECD of O-PB that are not attached to the electrodes.

fig. S9. PB thickness measurement.

fig. S10. Twenty times of CV scan (−0.05 to 0.35 V versus reference electrode at a scan rate of 50 mV/s).

fig. S11. Bode plot of O-Au, N-Au, O-PB, and N-PB scan frequency of 1×10^{-2} to 1×10^{-4} Hz.
fig. S12. Electrochemical characterization of the N-PB after 2 months' storage.
fig. S13. Mechanical property measurement of O-PB and N-PB.
fig. S14. Biosensing device calibration experiment of high-density glucose.
fig. S15. CV scan (−0.05 to 0.35 V versus reference electrode at a scan rate of 50 mV/s) of the device in four-time repeated glucose calibration experiments.
fig. S16. Influence of pH value and temperature change on device's performance.
fig. S17. Skin surface temperature measurement in 20 min at room temperature with a Pt temperature sensor.
fig. S18. Skin surface condition.
movie S1. ROSE transfer printing.

REFERENCES AND NOTES

1. B. B. Lowell, G. I. Shulman, Mitochondrial dysfunction and type 2 diabetes. *Science* **307**, 384–387 (2005).
2. D. A. Gough, L. S. Kumosa, T. L. Routh, J. T. Lin, J. Y. Lucisano, Function of an implanted tissue glucose sensor for more than 1 year in animals. *Sci. Transl. Med.* **2**, 42ra53 (2010).
3. S. K. Vashist, Non-invasive glucose monitoring technology in diabetes management: A review. *Anal. Chim. Acta* **750**, 16–27 (2012).
4. A. Tura, A. Maran, G. Pacini, Non-invasive glucose monitoring: Assessment of technologies and devices according to quantitative criteria. *Diabetes Res. Clin. Pract.* **77**, 16–40 (2007).
5. A. J. Bandodkar, W. Jia, J. Wang, Tattoo-based wearable electrochemical devices: A review. *Electroanalysis* **27**, 562–572 (2015).
6. M. G. Ghosn, N. Sudheendran, M. Wendt, A. Glasser, V. V. Tuchin, J. V. Larin, Monitoring of glucose permeability in monkey skin in vivo using optical coherence tomography. *J. Biophotonics* **3**, 25–33 (2010).
7. K. V. Larin, M. S. Eledrisi, M. Motamedi, R. O. Esenaliev, Noninvasive blood glucose monitoring with optical coherence tomography: A pilot study in human subjects. *Diabetes Care* **25**, 2263–2267 (2002).
8. H. Shibata, Y. J. Heo, T. Okitsu, Y. Matsunaga, T. Kawanishi, S. Takeuchi, Injectable hydrogel microbeads for fluorescence-based in vivo continuous glucose monitoring. *Proc. Natl. Acad. Sci. U.S.A.* **107**, 17894–17898 (2010).
9. O. K. Cho, Y. O. Kim, H. Mitsumaki, K. Kuwa, Noninvasive measurement of glucose by metabolic heat conformation method. *Clin. Chem.* **50**, 1894–1898 (2004).
10. X. Yang, A. Y. Zhang, D. A. Wheeler, T. C. Bond, C. Gu, Y. Li, Direct molecule-specific glucose detection by Raman spectroscopy based on photonic crystal fiber. *Anal. Bioanal. Chem.* **402**, 687–691 (2012).
11. R. K. Shervedani, A. H. Mehrjardi, N. Zamiri, A novel method for glucose determination based on electrochemical impedance spectroscopy using glucose oxidase self-assembled biosensor. *Bioelectrochemistry* **69**, 201–208 (2006).
12. W. Gao, S. Emaminejad, H. Y. Y. Nyein, S. Challa, K. Chen, A. Peck, H. M. Fahad, H. Ota, H. Shiraki, D. Kiriya, D.-H. Lien, G. A. Brooks, R. W. Davis, A. Javey, Fully integrated wearable sensor arrays for multiplexed in situ perspiration analysis. *Nature* **529**, 509–514 (2016).
13. A. Soni, S. K. Jha, A paper strip based non-invasive glucose biosensor for salivary analysis. *Biosens. Bioelectron.* **67**, 763–768 (2015).
14. S. Iguchi, H. Kudo, T. Saito, M. Ogawa, H. Saito, K. Otsuka, A. Funakubo, K. Mitsubayashi, A flexible and wearable biosensor for tear glucose measurement. *Biomed. Microdevices* **9**, 603–609 (2007).
15. H. Lee, T. K. Choi, Y. B. Lee, H. R. Cho, R. Ghaffari, L. Wang, H. J. Choi, T. D. Chung, N. Lu, T. Hyeon, S. H. Choi, D.-H. Kim, A graphene-based electrochemical device with thermoresponsive microneedles for diabetes monitoring and therapy. *Nat. Nanotechnol.* **11**, 566–572 (2016).
16. J. Heikenfeld, Non-invasive analyte access and sensing through eccrine sweat: Challenges and outlook circa 2016. *Electroanalysis* **28**, 1242–1249 (2016).
17. A. Koh, D. Kang, Y. Xue, S. Lee, R. M. Pielak, J. Kim, T. Hwang, S. Min, A. Banks, P. Bastien, M. C. Manco, L. Wang, K. R. Ammann, K.-I. Jang, P. Won, S. Han, R. Ghaffari, U. Paik, M. J. Slepian, G. Balooch, Y. Huang, J. A. Rogers, A soft, wearable microfluidic device for the capture, storage, and colorimetric sensing of sweat. *Sci. Transl. Med.* **8**, 366ra165 (2016).
18. H. Lee, C. Song, Y. S. Hong, M. S. Kim, H. R. Cho, T. Kang, K. Shin, S. H. Choi, T. Hyeon, D.-H. Kim, Wearable/disposable sweat-based glucose monitoring device with multistage transdermal drug delivery module. *Sci. Adv.* **3**, e1601314 (2017).
19. J. Kost, S. Mitragotri, R. A. Gabbay, M. Pishko, R. Langer, Transdermal monitoring of glucose and other analytes using ultrasound. *Nat. Med.* **6**, 347–350 (2000).
20. M. Pleitez, H. von Lilienfeld-Toal, W. Mäntele, Infrared spectroscopic analysis of human interstitial fluid in vitro and in vivo using FT-IR spectroscopy and pulsed quantum cascade lasers (QCL): Establishing a new approach to non invasive glucose measurement. *Spectrochim. Acta A Mol. Biomol. Spectrosc.* **85**, 61–65 (2012).
21. A. J. Bandodkar, W. Jia, C. Yardımcı, X. Wang, J. Ramirez, J. Wang, Tattoo-based noninvasive glucose monitoring: A proof-of-concept study. *Anal. Chem.* **87**, 394–398 (2015).
22. G. Rao, R. H. Guy, P. Glikfeld, W. R. LaCourse, L. Leung, J. Tamada, R. O. Potts, N. Azimi, Reverse iontophoresis: Noninvasive glucose monitoring in vivo in humans. *Pharm. Res.* **12**, 1869–1873 (1995).
23. A. Sieg, R. H. Guy, M. B. Delgado-Charro, Simultaneous extraction of urea and glucose by reverse iontophoresis in vivo. *Pharm. Res.* **21**, 1805–1810 (2004).
24. T. S. Ching, P. Connolly, Simultaneous transdermal extraction of glucose and lactate from human subjects by reverse iontophoresis. *Int. J. Nanomedicine* **3**, 211–223 (2008).
25. B. Leboulanger, R. H. Guy, M. B. Delgado-Charro, Reverse iontophoresis for non-invasive transdermal monitoring. *Physiol. Meas.* **25**, R35–R50 (2004).
26. Y. Chen, B. Lu, Y. Chen, X. Feng, Biocompatible and ultra-flexible inorganic strain sensors attached to skin for long-term vital signs monitoring. *IEEE Electron. Device Lett.* **37**, 496–499 (2016).
27. X. Feng, M. A. Meitl, A. M. Bowen, Y. Huang, R. G. Nuzzo, J. A. Rogers, Competing fracture in kinetically controlled transfer printing. *Langmuir* **23**, 12555–12560 (2007).
28. H. Chen, X. Feng, Y. Huang, Y. Huang, J. A. Rogers, Experiments and viscoelastic analysis of peel test with patterned strips for applications to transfer printing. *J. Mech. Phys. Solids* **61**, 1737–1752 (2013).
29. Y. Chen, B. Lu, Y. Chen, X. Feng, Breathable and stretchable temperature sensors inspired by skin. *Sci. Rep.* **5**, 11505 (2015).
30. J.-W. Jeong, W.-H. Yeo, A. Akhtar, J. J. S. Norton, Y.-J. Kwack, S. Li, S.-Y. Jung, Y. Su, W. Lee, J. Xia, H. Cheng, Y. Huang, W.-S. Choi, T. Bretl, J. A. Rogers, Materials and optimized designs for human-machine interfaces via epidermal electronics. *Adv. Mater.* **25**, 6839–6846 (2013).

Acknowledgments

Funding: We acknowledge the support from the National Basic Research Program of China (grant 2015CB351904) and National Natural Science Foundation of China (grants 11625207, 11222220, and 11320101001). We thank Tsinghua Nanofabrication Technology Center for material deposition and characterization. **Author contributions:** Y.C. and X.F. designed the experiments and wrote the paper. Y.C. and S.L. fabricated the device. Y.C. and S.Z. carried out the experiments and analysis. Y.L., Z.Q., Y.C., and B.L. provided theory support and supplied materials. X.W. supervised the clinical trial. All authors discussed the results and contributed to editing the manuscript. **Competing interests:** The authors declare that they have no competing interests. **Data and materials availability:** All data needed to evaluate the conclusions in the paper are present in the paper and/or the Supplementary Materials. Additional data related to this paper may be requested from the authors.

Submitted 16 May 2017
Accepted 27 November 2017
Published 20 December 2017
10.1126/sciadv.1701629

Citation: Y. Chen, S. Lu, S. Zhang, Y. Li, Z. Qu, Y. Chen, B. Lu, X. Wang, X. Feng, Skin-like biosensor system via electrochemical channels for noninvasive blood glucose monitoring. *Sci. Adv.* **3**, e1701629 (2017).